Solid-Solid Phase Transformation via Virtual Melting Significantly Below the Melting Temperature

Valery I. Levitas,[1] Bryan F. Henson,[2] Laura B. Smilowitz,[2] and Blaine W. Asay[2]
[1]*Center for Mechanochemistry and Synthesis of New Materials, Texas Tech University, Lubbock, Texas 79409, USA*
[2]*Los Alamos National Laboratory, Los Alamos, New Mexico 87545, USA*
(Received 5 August 2003; published 10 June 2004)

A new phenomenon is theoretically predicted, namely, that solid-solid transformation with a relatively large transformation strain can occur through virtual melting along the interface at temperatures significantly (more than 100 K) below the melting temperature. The energy of elastic stresses, induced by transformation strain, increases the driving force for melting and reduces the melting temperature. Immediately after melting, the stresses relax and the unstable melt solidifies. Fast solidification in a thin layer leads to nanoscale cracking, which does not affect the thermodynamics and kinetics of solid-solid transformation. Seven theoretical predictions are in quantitative agreement with experiments conducted on the $\beta \rightarrow \delta$ transformation in the HMX energetic crystal.

DOI: 10.1103/PhysRevLett.92.235702 PACS numbers: 64.70.Kb, 64.60.–i, 68.35.Rh

The main geometric characteristic of the phase transformation (PT) is the transformation strain tensor $\boldsymbol{\varepsilon}^t$, which transforms the unit cell of the parent phase 1 into the unit cell of the product phase 2. For a PT with a large $\boldsymbol{\varepsilon}^t$ and a coherent interface, a huge amount of the energy of the internal stresses can be accumulated during the PT. This energy reduces the driving force for the PT. Also, a moving interface between two solids experiences resistance due to the interaction with the stress field of crystal lattice defects. The elastic energy can be reduced (and the driving force can be increased) through various relaxation mechanisms, like dislocation generation and motion, twinning, and fracture [1,2]. The internal stresses and mechanism of their relaxation affect significantly the thermodynamics and kinetics of transformation and microstructure.

In this Letter, we predict virtual melting as an alternative mechanism of stress relaxation and loss of coherency at a moving solid-solid interface. If melting occurs along the interface, the elastic energy completely relaxes. This change in the elastic energy increases the driving force for melting, reduces melting temperature, and causes melting. Immediately after melting, stresses relax and unstable melt (m) crystallizes in a stable phase 2. The melt in each transforming material point exists during an extremely short time sufficient for stress relaxation, it is a transitional activated state rather than a real (thermodynamically stable) melt. We called this state the virtual melt, similar virtual austenite in the theory of the martensitic PT [3]. Fast solidification in a thin layer leads to nanoscale cracking, which does not affect thermodynamics and kinetics of the solid-solid PT. This process repeats itself at each interface increment. It is also found that nonhydrostatic compressive stresses promote melting in contrast to hydrostatic pressure. The theoretical predictions are quantitatively confirmed by seven experimental results on the $\beta \rightarrow \delta$ PT in the organic nitramine octahydro-1,3,5,7-tetranitro-1,3,5,7-tetrazocine (HMX) energetic crystal.

Thermodynamics.—As an initial configuration, we consider a plane incoherent interface AB between the phases 1 and 2 with no external and internal stresses (Fig. 1). It is also a good approximation of a small part of the curved interface. The change in molar Gibbs energy at zero stress $\Delta g_{1\rightarrow 2} < 0$ at a given temperature. Let us assume that the PT occurs in a thin layer V_n by propagation of the coherent interface CD from the position AB (Fig. 1). The incoherent interface AB is fixed and transforms to a grain boundary after the PT in a layer $ABCD$. This process can be considered a nucleation at the grain boundary (or incoherent interface). We also assume that there is no sliding along the fixed grain boundary AB, plasticity, and fracture; i.e., the elastic energy does not relax and is the same as for a coherent nucleus. Using the Eshelby solution for a penny-shaped ellipsoid with axes a

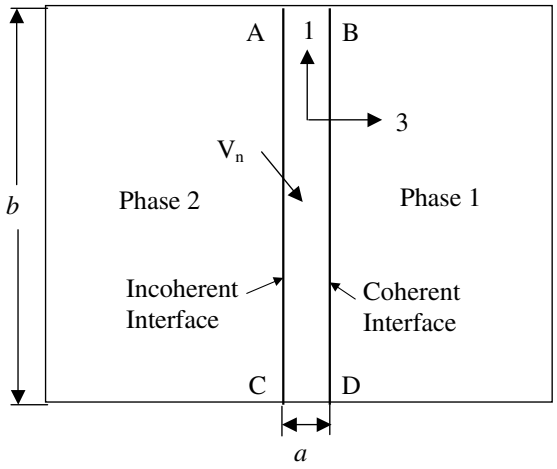

FIG. 1. Scheme of the solid-solid phase transformation $1 \rightarrow 2$ in the volume V_n through the intermediate melting.

and b and an aspect ratio $n = a/b \ll 1$ and neglecting all terms containing n, we derive for the elastic energy per mole [4]

$$g^e = \mu V[(\varepsilon^t_{11})^2 + (\varepsilon^t_{22})^2 + 2\nu\varepsilon^t_{11}\varepsilon^t_{22} + 2(1-\nu)(\varepsilon^t_{12})^2]/(1-\nu) > 0, \quad (1)$$

where μ is the shear modulus, ν is the Poisson's ratio (the same for phases 1 and 2, which does not change any conclusion), and V is the molar volume. Components of $\boldsymbol{\varepsilon}^t$ deforming the interface (Fig. 1) contribute to g^e only. After melting, the interface is incoherent, and the elastic energy is proportional to n (see [4]), i.e., is negligible in comparison with g^e.

The thermodynamic criterion for the solid-solid PT in the elastic material reads [1,5] $F^c_{1\to 2} = -g^e - \Delta g_{1\to 2} - K - V(\Gamma_{gb} + \Gamma_c - \Gamma_{in})/a \geq 0$, where F is the net driving force for the PT per mol; K is the athermal dissipation due to the PT mostly related to interface friction and caused by a long range stress field of defects; Γ_{gb}, Γ_c, and Γ_{in} are the grain boundary, coherent interface energy, and incoherent interface energy, and the superscript c denotes coherent. The elastic energy reduces the driving force for the PT $1 \to 2$ and suppress the PT. For the melting $F_{2\to m} = g^e - \Delta g_{2\to m} - V\Delta\Gamma_{2-m}/a \geq 0$, where $\Delta\Gamma_{2-m} = \Gamma_{2-m} + \Gamma_{1-m} - \Gamma_{gb} - \Gamma_c$ and Γ_{i-m} is the phase i-m interface energy. We put $K = 0$, because liquid, as the hydrostatic medium, does not interact with the stress field of crystal defects, consequently, the resistance to interface propagation is absent. The elastic energy before melting g^e disappears after melting, thus increasing the driving force for melting. For organic crystals, $\Gamma_{i-m} = (0.15 - 0.3)\Gamma_{gb}$, for metals $\Gamma_{i-m} = (0.3 - 0.45)\Gamma_{gb}$ [1], and $\Delta\Gamma_{2-m} \leq 0$; i.e., there is no barrier for melt nucleation due to surface energy. To avoid lengthy size-dependent calculations, we put $\Delta\Gamma_{2-m} = 0$, decreasing the driving force for melting, which did not result in a change to the conclusions. It is known that allowing for $\Delta\Gamma_{2-m} \leq 0$ leads to a decrease in melting temperature by several degrees (premelting) [6]. From the phase equilibrium condition $F_{2\to m} = 0$, one determines how the melting temperature θ_m reduces as a result of the elastic energy

$$\theta^e_m = [\Delta h_{2\to m}(\theta^e_m) - g^e]/\Delta s_{2\to m}(\theta^e_m). \quad (2)$$

Generally, because the changes in enthalpy $\Delta h_{2\to m}$ and entropy $\Delta s_{2\to m}$ are functions of temperature, Eq. (2) is a nonlinear equation with respect to θ^e_m. The smaller $\Delta s_{2\to m}$ is and the larger g^e is, the larger $\theta_m - \theta^e_m$ is.

Note that for tensile $\varepsilon^t_{ii} > 0$, compressive stresses in V_n are generated after $1 \to 2$ PT. Because in most cases, melting is accompanied by volumetric expansion $\varepsilon^m_0 > 0$, thermodynamics and experiment exhibit growth of the melting temperature with increasing pressure, which appears to be in contradiction to our results. The solution is in the nonhydrostatic stresses and transformation strains. It can be shown, based on [4], that the transformation strains along the interface with respect to phase 2 for melting $\varepsilon^m_{ii} = n\varepsilon^m_0\pi(1-2\nu)/[8(1+\nu)] - \varepsilon^t_{ii}$; here $i = 1, 2$. Condition $n \ll 1$ implies $\varepsilon^m_{ii} < 0$, i.e., during melting, compression occurs along the interface and compressive stresses σ_{11} and σ_{22} promote melting. In orthogonal to the interface direction, transformation strain during melting is, of course, tensile. However, stress σ_{33} is proportional to n and is negligible in comparison with σ_{11} and σ_{22}; see [4]. As it follows from Eq. (1), the elastic energy is always positive, and if ε^t_{11} and ε^t_{22} have the same sign, it is independent of the sign of the transformation strains.

Solidification and nanocracking.—After melting, internal stresses relax and unstressed melt is unstable with respect to solid phase 2, because at $\theta^e_m < \theta_m$, $F_{m\to 2} = -\Delta g_{m\to 2} > 0$. We assume that during solidification of a thin liquid layer, the layer has a complete adhesion to the solid phases. Then the solidification generates compressive equiaxial transformation strains $\varepsilon^s_{ii} = \varepsilon^s_0/3 < 0$, where $i = 1, 2, 3$, ε^s_0 is the volumetric transformation strain during solidification. Using the Eshelby solution [4] and neglecting the terms with n, one obtains $\sigma_{11} = \sigma_{22} = -E\varepsilon^s_0/[3(1-\nu)] > 0$, and all other stresses are zero, where E is Young's modulus. In the elastic regime, these tensile stresses cause tensile elastic strains $\varepsilon^e_{11} = \varepsilon^e_{22} = \sigma_{11}(1-\nu)/E = -\varepsilon^s_{11}$ and compressive elastic strain $\varepsilon^e_{33} = -2\nu\sigma_{11}/E$. During solidification, the yield stress and the maximal normal tensile stress (resistance to fracture) are negligible. That is why we assume that the elastic strains ε^e_{11} and ε^e_{22} completely relax through one or more of these mechanisms: vacancies' generation, microcracking, cavitation; i.e., the inelastic strain due to cracking is $\varepsilon^c_{11} = \varepsilon^c_{22} = \varepsilon^e_{11} = -\varepsilon^s_{11}$. This leads to the complete relaxation of stresses σ_{11} and σ_{22} and consequently the compressive strain ε^e_{33}. The volumetric strain due to cracking $\varepsilon^c_0 = 2\varepsilon^c_{11} = -2\varepsilon^s_0/3 > 0$, which is the upper bound for the porosity induced by this mechanism. The characteristic size of the initial microcavities is $\sim a$, i.e., of nm size. However, as cracking occurs sequentially in the whole transforming volume, the size can grow by diffusion and coalescence, because the temperature is high enough.

As it follows from the theory of the PT in inelastic materials [2] (which includes dislocation plasticity and fracture), the inelastic process of the appearance of microcavities does not contribute to the driving force for the $1 \to 2$ PT directly, only though the stress variation. As the stresses before and after the $1 \to 2$ PT are zero, the stress (and the elastic energy) change is zero as well. Each inelastic process has its own driving force independent of the driving force for the PT. In the given case, internal stresses cause damage when resistance to damage is close to zero. Consequently, the appearance of microcavities does not affect the driving force for the $1 \to 2$ PT, which was an unexpected result.

Kinetics.—Without the relaxation of the elastic energy, it makes a negative contribution to the driving force $F_{1\to 2}$. If it relaxes via virtual melting, the net driving

force $F_{1\to2} = -\Delta g_{1\to2}$ (there is no change in interface energy), elastically stressed coherent phase 1, and melt are activated states (Fig. 2). We did not include K, because the coherent phase 2 activated state is not supposed to be subjected to dry interface friction. The interface velocity can be presented in the form $v = v_0\{\exp[-E_{1\to2}/(R\theta)] - \exp[-E_{2\to1}/(R\theta)]\}$, where v_0 is the preexponential factor, $E_{1\to2}$ and $E_{2\to1}$ are the activation energies for the $1 \to 2$ and $2 \to 1$ PTs, and R is the gas constant. Condition $F_{2\to m} = 0$ results in $g_2^e = \Delta g_{2\to m}$. According to Fig. 2, $E_{1\to2} = \Delta g_{2\to m} + \Delta g_{1\to2} = \Delta g_{1\to m}$ and $E_{2\to1} = \Delta g_{2\to m}$. Thus,

$$v = v_0 \exp\left(\frac{\Delta s_{2\to m}}{R}\right)\exp\left(-\frac{\Delta h_{2\to m}}{R\theta}\right)\left[\exp\left(-\frac{\Delta g_{1\to2}}{R\theta}\right)-1\right]. \quad (3)$$

In the same way, the same result with a different preexponential factor was obtained for the rate constant in the kinetic equation for a volume fraction of the phase 2. The temperature dependence of the rate constant is determined by the heat of fusion $h_{2\to m}$.

Experimental validation.—To prove the validity of the virtual melting, we consider the $\beta \to \delta$ PT in the organic HMX energetic crystal [7,8]. Equation (3) basically coincides with Eq. (13) in [7]. Our activation energies, $E_{1\to2} = \Delta g_{1\to m}$ and $E_{2\to1} = \Delta g_{2\to m}$, coincide with activation energies postulated and experimentally confirmed in [7]. The temperature dependence of the rate constant is determined by the heat of fusion $h_{2\to m}$, as in experiments and in Eq. (13) in [7].

Let us estimate whether virtual melting can occur at $\beta - \delta$ phase equilibrium temperature 430 K, which is by 121 K lower than the melting temperature of δ phase $\theta_m = 551$ K. Taking data from [9] for $\theta = 430$ K for the δ phase and extrapolating data from [9] for melt, we obtain $\Delta s_{\delta\to m} = 132.83$ J/mol K, $\Delta h_{\delta\to m} = 66\,188.3$ J/mol, and the elastic energy g^e necessary to fulfill melting criterion Eq. (2) is $g^e = 9.072$ kJ/mol. We use the molecular weight $M \simeq 0.296$ kg/mol and the mass density $\rho = 1650$ kg/m^3 [10], $V = M/\rho = 1.8 \times 10^{-4}$ m^3/mol, $\mu = 6.925$ GPa (estimated for the bulk modulus $B \simeq 15$ GPa [10] and $\nu = 0.3$). The actual mechanism of transformation of the monoclinic β phase into hexagonal δ phase is unknown, and the only one known is the volumetric transformation strain $\varepsilon_0 \simeq 0.08$. We assume $\varepsilon_{11}^t = \varepsilon_{22}^t = 1/2\varepsilon_{21}^t$, and find the value ε_{11}^t required for melting from the condition $g^e = 9.072$. The obtained value $\varepsilon_{11}^t = 0.025$ is reasonable because it is smaller than $\varepsilon_0/3 = 0.027$.

Note that at $\theta_m = 551$ K, the experimental value $\Delta h_{\delta\to m} = 69.9 \pm 4.2$ kJ/mol [9]. Calculations in [7] and here are based on $\Delta h_{\delta\to m} = 69.9$ kJ/mol. The indeterminacy in the enthalpy change is approximately half of the required elastic energy. If we take the lower bound for $\Delta h_{\delta\to m}$ and subtract 4.2 kJ/mol from the required elastic energy, we obtain $\varepsilon_{11}^t = 0.018$.

Considerable cracking, homogeneously distributed in the transformed material over the 500 nm scale accompanies the PT (Fig. 3), as predicted by theory. However, without virtual melting, stresses in the V_n are compressive and cannot cause the nanocracking. Macroscopic cracks [Fig. 3(b)] are caused by tensile stresses in the β matrix due to volumetric transformation expansion in δ inclusions. Tensile macrostresses follow from the elastic solution even for a completely incoherent interface; i.e., they do not contradict the virtual melting along the interface. The nanocracking does not change the PT thermodynamics and kinetics appreciably [8], as predicted by theory.

Note that for $382.4 < \theta < 430$, the orthorhombic α phase is stable; i.e., the $\beta \to \alpha$ PT is expected to occur, but does not. Because $\varepsilon_0^{\beta\to\alpha} \simeq 0.5\varepsilon_0^{\beta\to\delta}$, g^e and the decrease in melting temperature is 4 times smaller; i.e., virtual melting cannot occur. The lack of the $\beta \to \alpha$ PT demonstrates that other stress relaxation mechanisms are not efficient or increase K, as plasticity and fracture usually do [2]. At $\theta = 430.6$, the value $-\Delta g_{\beta\to\alpha} = 760$ J/mol [11] characterizes the value $K + g^e$ for the $\beta \to \alpha$ PT under actual mechanisms of stress relaxation.

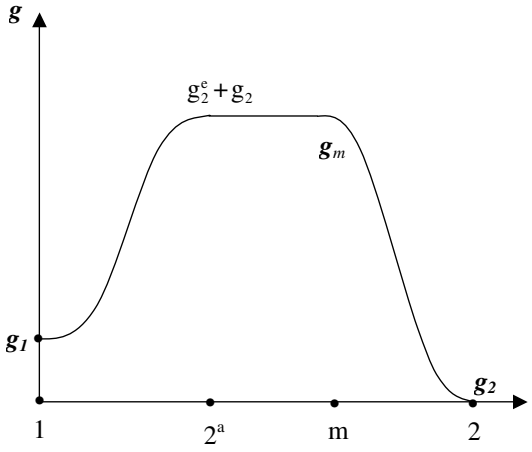

FIG. 2. Change in the Gibbs energy along the transformation path $1 \to 2$ through elastically stressed phase 2^a and virtual melt m, which are transitional activated states.

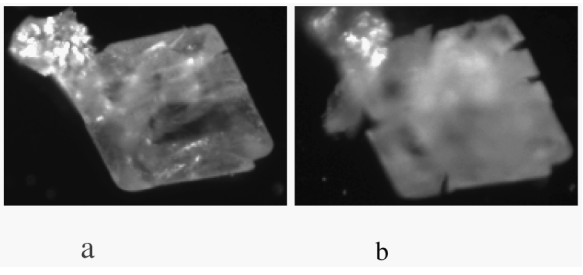

FIG. 3. Transparent β-phase HMX crystal (a) and opaque δ-phase crystal (b) after the $\beta - \delta$ PT. The opaqueness is caused by cracks distributed at the scale of 500 nm. Without virtual melting, only macroscopic cracks are expected.

As the threshold K is proportional to ε_0 [2], it should be 2 times smaller than for the $\beta \rightarrow \delta$ PT. In experiment the $\beta \rightarrow \delta$ PT begins at 430.6 K, i.e., immediately above the equilibrium temperature $\theta^e = \Delta h_{\beta\rightarrow\delta}/\Delta s_{\beta\rightarrow\delta} = 9800/22.76 = 430.58$ [7]; that implies $K \simeq g^e \simeq 0$, which is very unusual for the solid-solid PT. This is possible for the PT through liquid only, because other relaxation mechanisms (dislocation and crack generation) increase K. Taking $K + g^e = 760$ J/mol, the lower bound for $\theta_{\beta\rightarrow\delta} = 464$ K in the absence of melting can be obtained.

Note that our experiments [7,8] were conducted at $\theta < 448$ at which the thermal decomposition of HMX and impurities is excluded. It was confirmed by optical microscopy and Raman spectroscopy. The PT was also cycled several times for the same sample with the same kinetics.

To summarize, there are the following coincidences of the predicted and observed: (1) a decrease in melting temperature (121 K); (2) activation energies for the direct and the reverse PT, which are equal to the corresponding melting energy ($E_{1\rightarrow2} = \Delta g_{1\rightarrow m}$ and $E_{2\rightarrow1} = \Delta g_{2\rightarrow m}$); (3) temperature dependence of the rate constant determined by the heat of fusion $h_{2\rightarrow m}$; (4) $K \simeq g^e \simeq 0$ (in contrast to all known solid-solid PTs); (5) nanoscale cracking; (6) independence of thermodynamics and kinetics of the solid-solid PT of the nanoscale cracking, and (7) the absence of the $\beta \rightarrow \alpha$ PT. Because it is difficult to imagine any other mechanism that explains all these experimental results, we conclude that the $\beta \rightarrow \delta$ PT in the HMX crystal occurs through virtual melting.

Note that if a stressed layer V_n is formed and melting can occur, some other relaxation mechanisms are suppressed. If stresses are compressive (as for HMX), cracks cannot appear. For tensile stresses, crack nucleation is possible in the direction orthogonal to tensile stresses. However, if a is smaller than the critical crack length under a given stress field, the crack cannot nucleate, but melting can occur. Additionally, a crack in thin layer releases the elastic energy only in some of the volume surrounding the crack, roughly in the region of a. So, a huge number of cracks are necessary to release the entire elastic energy. This occurs in the thin layer during the solidification.

From strained epitaxial film research, we know that dislocation nucleates at some critical width of the films when critical stored energy is accumulated [12]. For some systems, melting can occur at smaller thicknesses. The appearance of dislocation decreases the total elastic energy of the layer, but increases the local elastic energy in the small vicinity of dislocation, which promotes the nucleation of the melt. In organic materials with complex molecules and relatively large cell parameters (like HMX), the nucleation of dislocation is naturally suppressed as a result of their high energy.

Thus, we found a new mechanism of the solid-solid PT, the loss of interface coherency, and the stress relaxation via virtual melting. The mechanism significantly changes thermodynamics (increases $F_{1\rightarrow2}$ up to $g_{1\rightarrow2}$ and eliminates K) and kinetics (activation energy) of the solid-solid PT and leads to nanocracking. This mechanism can be operative for material systems, for which (a) the reduction in melting temperature due to the elastic energy exceeds the difference between the melting temperature and the solid-solid PT temperature and (b) the plasticity and fracture are suppressed. In particular, complex organic crystalline systems for which plasticity is suppressed (e.g., due to large Burgers vector) and polymorphs that are connected by the reconstructive PT with large transformation strain are good candidates. If a pressure-temperature phase diagram contains the triple 1-2-m point, then change in pressure, which makes $\theta_{1\text{-}2}$ and $\theta_{2\text{-}m}$ closer, renders the virtual melting the leading mechanism of the solid-solid PT for the majority of material systems with suppressed plasticity.

An alternative mechanism of stress relaxation during melt crystallization is an amorphization. A nanometer sized amorphous layer was observed for the PTs from cubic boron nitride (BN) to hexagonal BN and back ($\varepsilon_0 = 0.53$) near the triple point [13]. It was not explained in [13] by any known reasons, but can be explained by virtual melting.

V. I. L. acknowledges the support of NSF (CMS-02011108). B. F. H., L. B. S., and B. W. A. acknowledge the support of the Laboratory Research and Development and H.E. Science Programs at Los Alamos National Laboratory.

[1] D. A. Porter and K. E. Easterling, *Phase Transformation in Metals and Alloys* (Van Nostrand Reinhold, New York, 1992).
[2] V. I. Levitas, Int. J. Solids Struct. **35**, 889 (1998).
[3] V. I. Levitas and D. L. Preston, Phys. Rev. B **66**, 134207 (2002).
[4] T. Mura, *Micromechanics of Defects in Solids* (Martinus Nijhoff Publishers, Dordrecht, 1987).
[5] V. I. Levitas, Int. J. Plasticity **16**, 805 (2000); **16**, 851 (2000).
[6] D. M. Zhu and J. G. Dash, Phys. Rev. Lett. **57**, 2959 (1986).
[7] B. F. Henson *et al.*, Phys. Rev. Lett. **82**, 1213 (1999); B. F. Henson *et al.*, J. Chem. Phys. **117**, 3780 (2002).
[8] L. Smilowitz *et al.*, J. Chem. Phys. **117**, 3789 (2002).
[9] J. L. Lyman, Y. C. Liau, and H. V. Brand, Combust. Flame **130**, 185 (2002).
[10] R. Menikoff and T. D. Sewell, Combust. Theory Modell. **6**, 103 (2002).
[11] A. S. Teetsov and W. C. McCrone, Microsc. Cryst. Front **15**, 13 (1965); T. B. Brill and R. J. Karpowicz, J. Phys. Chem. **86**, 4260 (1982).
[12] A. D. Bukhovski, B. L. Gelmont, and M. S. Shur, J. Appl. Phys. **78**, 3691 (1995).
[13] M. I. Eremets *et al.*, Phys. Rev. B **57**, 5655 (1998).